J. Appl. Comput. Mech., 7(3) (2021) 1649-1662
DOI: 10.22055/JACM.2021.36566.2869

ISSN: 2383-4536
jacm.scu.ac.ir

Shahid Chamran University of Ahvaz

Journal of Applied and Computational Mechanics

Research Paper

Stability Analysis of Articulated Bus in Straight-ahead Running Manoeuvre

Alessandro De Felice[1], Matteo Mercantini[2], Silvio Sorrentino[3]

[1] Department of Engineering *Enzo Ferrari*, University of Modena and Reggio Emilia, Via Vivarelli 10, Modena, 41125, Italy, Email: alessandro.defelice@unimore.it

[2] Protezioni Elaborazioni Industriali (PEI) Srl, Via Torretta 32, Calderara di Reno, 40012, Italy, Email: mmercantini@pei.it

[3] Department of Engineering *Enzo Ferrari*, University of Modena and Reggio Emilia, Via Vivarelli 10, Modena, 41125, Italy, Email: silvio.sorrentino@unimore.it

Received January 05 2021; Revised March 22 2021; Accepted for publication March 22 2021.
Corresponding author: S. Sorrentino (silvio.sorrentino@unimore.it)

Abstract. A comprehensive study on the stability of a planar linearized single-track model of a two-section pusher articulated bus is presented with the aid of a complete set of stability maps. The two sections of the vehicle model are connected at the hitch point by a revolute joint; an equivalent visco-elastic characteristic function describes its rotational visco-elastic properties, playing a major role in stability control and therefore in passive safety. The equations of motion are derived in analytical form, allowing easy implementation of the non-linear model (eventually including a non-linear viscoelastic characteristic functions of the joint). Stability of the linearized model is then studied in equilibrium configurations by means of sensitivity analysis with respect to the model's governing parameters. Stability maps are drawn on the basis of sets of parameter values related to straight-ahead running, steady-state manoeuvres. The most important parameters controlling the onset of unstable motions are identified, paying attention to the role played by the equivalent rotational damping coefficient and the equivalent torsional stiffness characterizing the connection joint, with the aim of finding criteria for its design.

Keywords: Pusher articulated bus, hydraulic joint, single-track model, stability analysis, Hurwitz criterion, yaw instability, jackknifing.

1. Introduction

Design of city buses is a topic of interest in current research, both in terms of control [1] and sustainable mobility [2]. As for articulated buses, stability control is an issue of great practical importance, since the onset of unstable oscillations like 'jackknifing' can lead to loose of control, and to dangerous accidents. The basic purpose of stability control functions, which in EU are mandatory since 2014, is to prevent roll-over and yaw instability [3], for which experimental testing procedures have been set more than thirty years ago [4].

In this context, stability of pusher articulated buses, having the engine mounted at the rear of the trailer, is a relevant problem. In this very common kind of city buses, passive control of 'jackknifing' is usually pursued by introducing a specifically designed hydraulic joint at the connection between the two sections of the vehicle [5]. Therefore, for improving design and control effectiveness, stability analysis must be conducted by investigating the effects of all the influential parameters on lateral dynamics, in connection with those characterizing the hydraulic joint.

Several contributions can be found in the literature dealing with different aspects of stability of articulated vehicles. A state of the art study on directional performance issues in design of articulated heavy vehicles (mainly devoted to trucks) is presented in [6], with an overview of the models used in designing controllers. Among the conclusions, it is herein worth mentioning the large influence due to different types of hitching elements employed at the articulation points. In [7] a single-track model of an articulated vehicle (with no damping at the revolute joint) is developed and then linearized for studying its stability by means of eigenvalue analysis. In [3] the main aim is to understand the fundamental differences between the dynamic yaw performance of truck-trailer combinations in vehicles with multiple articulations; since rearward amplification was recognised as a discriminatory performance measure, a frequency domain approach is adopted to study the fundamental differences between vehicle combinations. A stability map of a simplified linearized single-track model is displayed in [8], obtained by applying the Routh-Hurwitz criterion [9], while in [10] the analysis is focused on the effects of a particular tyre model (delayed tyre model), showing stability maps constructed with respect to the vehicle longitudinal velocity and the payload position on the trailer. The effects of interaction between a driver and a car-trailer combination in straight-line motion is investigated in [11], displaying stability maps as functions of speed and of a parameter giving a measure of the interaction of the driver. Moreover, the analysis presented in [12] is focused on understanding whether a truck-trailer system after loss of stability of the steady state still is controllable by the driver or not. Another simplified model (5 dofs), with nonlinear tyres, is presented in [13] for analyzing the stability of a tractor-semitrailer in lane changes under rainy weather.

Published online: March 24 2021

Besides [11, 12, 13], a very few other studies deal with non-linear analysis, in all cases considering simplified models of a tractor-trailer vehicle. In [14] it is shown that varying the travelling speed, only two kinds of instability can occur: either a divergence or a Hopf bifurcation. By means of bifurcation analysis it is shown that the system in any case possesses a critical post-bifurcation behaviour, meaning that the motion of the vehicle can become unstable even in the linearly stable domain of the driving speed, if a perturbation is large enough. The modes that can become unstable are identified in [15], by applying bifurcation analysis: 'jackknifing' (main component given by relative rotation angle with the trailer), 'sideslip' (main component given by the sideslip angle, i.e. by the lateral velocity component, in case of constant forward speed) and 'spinning' (main component given by the yaw rate). In [15] it is also shown that no unstable equilibrium point exists when the steering input is very small, and that yaw planar instability of a tractor semi-trailer can be caused by lateral tyre force saturation of the tractor's rear axles and/or the trailer's axles. A few other studies focus on more specific control problems on tractor semi-trailers, as for instance active steering [16] or 'jackknifing' control during high-speed curve driving [17].

Finally, some studies are specifically devoted to articulated buses (and in particular to pusher articulated buses), however presenting numerical simulations only of particular manoeuvres, using a single-track model [18, 19, 20]. In the analysis presented in [16], either a device with pure viscous friction or a device with dry friction are introduced at the connection joint with the trailer: this is the only contribution, besides [7, 11] and among those reported in the reference list, to take into account dissipative effects in the joint; while [11] is the only contribution considering also a rotational spring restraining the revolute joint.

This contribution consists of a comprehensive study on the linear stability of an articulated pusher bus with hydraulic joint, thoroughly investigated by means of a set of stability maps, which analysis to the best of the authors' knowledge is still missing in the literature. Though stability maps could be obtained adopting full vehicle multibody models [21, 22], in the present study they are drawn on the basis of a minimal (or essential) model, however able to include all the relevant parameters for a given manoeuvre. Therefore a planar single-track model of a two-section articulated bus is considered, characterized by the particular features of having the driving wheels on the single-axle trailer (with engine mounted at the rear of the trailer, affecting significantly the position of its center of mass), and a passive hydraulic joint connecting the two sections of the vehicle. The model consists of two rigid bodies (front section and rear section, i.e. trailer, with one axle) and four independent dofs; the two sections are connected at the hitch point by a revolute joint; an equivalent visco-elastic characteristic function describes the rotational visco-elastic properties of the connection joint, playing a major role in stability control. Through this function it is possible to include in the model different kinds of joints (hitch connections), or modifications in their design, or even different operational conditions. In particular, in this case the equivalent visco-elastic characteristics of a hydraulic joint are considered, as typically adopted in pusher articulated buses.

The paper is organized as follows: in Section 2 the single-track model is described, deriving its equations of motion in analytical form, allowing easy implementation of the characteristics of the joint; in Section 3 stability of the linearized model is studied in equilibrium configurations by means of sensitivity analysis with respect to the model's governing parameters; stability maps are drawn on the basis of sets of parameter values related to straight-ahead running, steady-state manoeuvres; the results are compared with those obtained using a multibody model of the vehicle; finally, the effects of the most influential parameters, including the role played by the joint, are discussed in Section 4.

2. Single-track model

The equations of motion of a planar single-track model of a two-section articulated bus (Fig. 1*a*,*b*) are analytically derived, first in non-linear form, then in their linearized form.

2.1 Description of the model

A planar single-track model is considered, consisting of two rigid bodies (front section and rear section, i.e. trailer, with one axle) connected by a revolute joint (pivot), with four independent dofs (two orthogonal displacements of the center of mass G_F of the front section, yaw angle ψ of the front section, and relative angle ϑ with respect to the trailer). In Fig. 1*b*, δ represents the steering angle of the front wheels, l_F the wheelbase of the front section (with a_F and b_F partial wheelbases), d the distance between G_F and pivot, G_R the center of mass of the trailer, l_R the distance between pivot and the trailer axle, a_R the distance between pivot and G_R, b_R the distance between G_R and the trailer axle, t_R the track of the trailer.

2.2 Slip angles at the wheels of the trailer

According to the schematic representation given in Fig. 1*b*, the absolute position of the ground contact point of the left wheel of the trailer can be written as:

$$\begin{Bmatrix} X_P \\ Y_P \end{Bmatrix} = \begin{Bmatrix} X_{G_F} - d\cos\psi - l_R\cos(\psi-\vartheta) - (t_R/2)\sin(\psi-\vartheta) \\ Y_{G_F} - d\sin\psi - l_R\sin(\psi-\vartheta) + (t_R/2)\cos(\psi-\vartheta) \end{Bmatrix} \tag{1}$$

where (X_{GF}, Y_{GF}) are the co-ordinates of the center of mass G_F in the inertial reference system (X, Y). If u, v are the longitudinal (direction x_F) and lateral (direction y_F) velocity components of point G_F, respectively, then the velocity of P can be expressed in a reference system fixed on the trailer and positioned on its longitudinal symmetry axis (x_R, y_R):

$$\begin{Bmatrix} u_{RP} \\ v_{RP} \end{Bmatrix} = \begin{Bmatrix} u\cos\vartheta - v\sin\vartheta + d\dot{\psi}\sin\vartheta - (t_R/2)(\dot{\psi}-\dot{\vartheta}) \\ u\sin\vartheta + v\cos\vartheta - d\dot{\psi}\cos\vartheta - l_R(\dot{\psi}-\dot{\vartheta}) \end{Bmatrix} \tag{2}$$

where u_{RP} and v_{RP} are the velocity components of P in direction x_R and y_R, respectively. Consequently, the slip angle at the left wheel (say α_{Rlw}) is defined by:

$$\tan(\alpha_{Rlw}) = -\left(\frac{v_{RP}}{u_{RP}}\right) = -\left[\frac{u\sin\vartheta + v\cos\vartheta - d\dot{\psi}\cos\vartheta - l_R(\dot{\psi}-\dot{\vartheta})}{u\cos\vartheta - v\sin\vartheta + d\dot{\psi}\sin\vartheta - (t_R/2)(\dot{\psi}-\dot{\vartheta})}\right] \tag{3}$$

which, if u prevails on the other velocity components, can be approximated as:

$$\alpha_{Rlw} \cong -\left[\frac{v}{u} - \left(d + \frac{l_R}{\cos\vartheta}\right)\frac{r}{u} + l_R\frac{s}{u\cos\vartheta} + \tan\vartheta\right] \quad \text{with} \quad r = \dot{\psi}, \quad s = \dot{\vartheta} \tag{4}$$

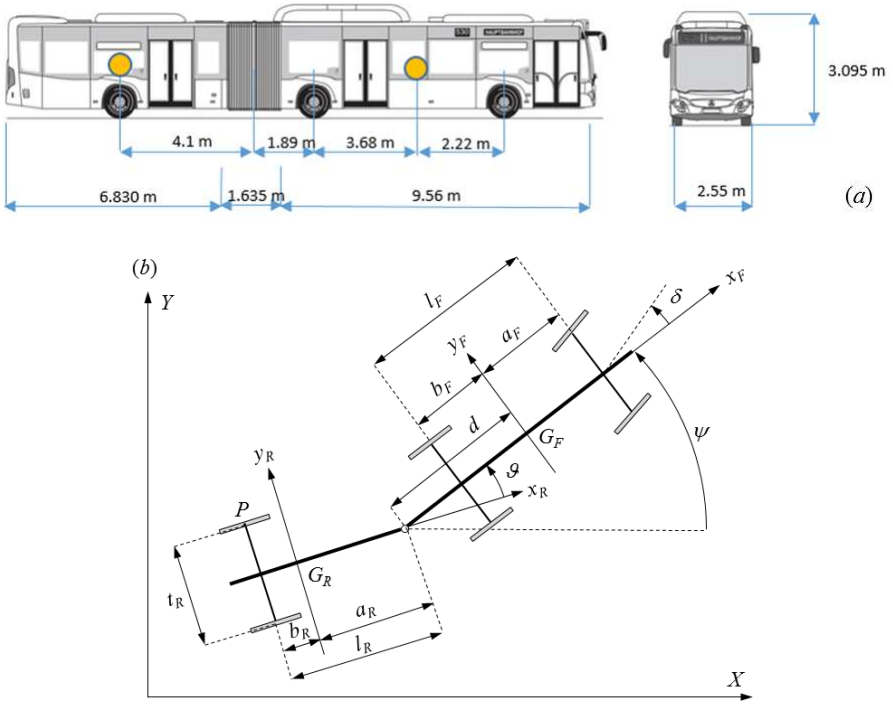

Fig. 1. Articulated bus under study, Mercedes-Benz Citaro G NGT 3 (*a*), and its schematic representation as a planar single-track – 4 dofs model (*b*).

In the last expression t_R vanishes, then it can be assumed that the two slip angles of the trailer axle are almost coincident, i.e. $\alpha_{Rlw} \cong \alpha_{Rrw} = \alpha_R$. In the case of straight-ahead running manoeuvres ($\vartheta \cong 0$), eq. (4) reduces to:

$$\alpha_R \cong -\frac{1}{u}\left[v-(d+l_R)r+l_R s\right]-\vartheta \tag{5}$$

which will be used in the linearized models, assuming constant values for u.

2.3 Equations of motion

The kinetic energy T of the 4 dofs planar model represented in Fig. 1*b* can be written in the form:

$$T=\frac{1}{2}m(\dot{X}^2+\dot{Y}^2)+m_R\left[d\dot{\psi}+a_R(\dot{\psi}-\dot{\vartheta})\cos\vartheta\right](\dot{X}\sin\psi-\dot{Y}\cos\psi)-m_R a_R\sin\vartheta(\dot{\psi}-\dot{\vartheta})(\dot{X}\cos\psi-\dot{Y}\sin\psi)+\frac{1}{2}J_1\dot{\psi}^2-J_2\dot{\vartheta}\dot{\psi}+\frac{1}{2}J_3\dot{\vartheta}^2 \tag{6}$$

where $\dot{X}$, $\dot{Y}$ are the absolute velocity components of G_F, and:

$$\begin{aligned}
&m=m_F+m_R\\
&J_1=J_1(\vartheta)=J_F+J_R+m_R(d^2+a_R^2+2da_R\cos\vartheta)\\
&J_2=J_2(\vartheta)=J_R+m_R(a_R^2+da_R\cos\vartheta)\\
&J_3=J_R+m_R a_R^2
\end{aligned} \tag{7}$$

Applying Lagrange equations yields:

$$\begin{cases}
m(\dot{u}-v\dot{\psi})-m_R a_R(\ddot{\psi}-\ddot{\vartheta})\sin\vartheta-2m_R a_R\dot{\psi}\dot{\vartheta}\cos\vartheta+m_R a_R\dot{\vartheta}^2\cos\vartheta+m_R(d+a_R\cos\vartheta)\dot{\psi}^2=Q_x\\
m(\dot{v}+u\dot{\psi})-m_R(d+a_R\cos\vartheta)\ddot{\psi}+m_R a_R\ddot{\vartheta}\cos\vartheta-m_R a_R(\dot{\psi}-\dot{\vartheta})^2\sin\vartheta=Q_y\\
J_1\ddot{\psi}-J_2\ddot{\vartheta}+m_R a_R d(\dot{\vartheta}^2-2\dot{\vartheta}\dot{\psi})\sin\vartheta-m_R(d+a_R\cos\vartheta)(\dot{v}+u\dot{\psi})-m_R a_R(\dot{u}-v\dot{\psi})\sin\vartheta=Q_\psi\\
J_3\ddot{\vartheta}-J_2\ddot{\psi}+m_R a_R(\dot{v}+u\dot{\psi})\cos\vartheta+m_R a_R(\dot{u}-v\dot{\psi})\sin\vartheta+m_R a_R d\dot{\psi}^2\sin\vartheta=-c\dot{\vartheta}-k\vartheta+Q_\vartheta
\end{cases} \tag{8}$$

where the Qs denote the generalized forces, while c and k are the rotational damping coefficient and the torsional stiffness at the pivot, respectively (obtained from a linearized viscoelastic characteristic function of the joint). In particular, recalling eqs. (2), the virtual displacement of the ground contact point of the left wheel of the trailer reads:

$$\begin{cases}
\delta x_{Rlw}=\delta x_F\cos\vartheta-\delta y_F\sin\vartheta+\delta\psi d\sin\vartheta-(t_R/2)(\delta\psi-\delta\vartheta)\\
\delta y_{Rlw}=\delta x_F\sin\vartheta+\delta y_F\cos\vartheta-\delta\psi d\cos\vartheta-l_R(\delta\psi-\delta\vartheta)
\end{cases} \tag{9}$$

At the right wheel the only difference would be the opposite sign before ($t_R/2$). Then, in case of non-steering wheels at the trailer, the virtual work done by the ground force components at the left wheel (F_{x31} and F_{y31}) is given by:

$$\delta L=(F_{x31}\cos\vartheta+F_{y31}\sin\vartheta)\delta x_F+(-F_{x31}\sin\vartheta+F_{y31}\cos\vartheta)\delta y_F+\left[F_{x31}[d\sin\vartheta-(t_R/2)]-F_{y31}(d\cos\vartheta+l_R)+M_{z31}\right]\delta\psi+\left[F_{x31}(t_R/2)+F_{y31}l_R-M_{z31}\right]\delta\vartheta \tag{10}$$

Table 1. List of parameters of the 4 dofs model.

Front section parameters	
Maximum number of passengers	$N_F = 87$
Mass (empty and full)	$m_F = 15873 \rightarrow 22398$ kg
Moment of inertia (empty and full)	$J_F = 136000 \rightarrow 190000$ kgm^2
Wheelbase	$l_F = 5.90$ m
Front wheelbase	$a_F = 2.22$ m
Rear wheelbase	$b_F = 3.68$ m
Distance between center of mass and pivot	$d = 5.57$ m
Front axle cornering stiffness	$C_1 = 166$ kN/rad
Rear axle cornering stiffness	$C_2 = 120$ kN/rad
Rear section parameters	
Maximum number of passengers	$N_R = 71$
Mass (empty and full)	$m_R = 12127 \rightarrow 17452$ kg
Moment of inertia (empty and full)	$J_R = 57000 \rightarrow 81000$ kgm^2
Distance between pivot and axle	$l_R = 4.10$ m
Distance between pivot and center of mass	$a_R = 4.10$ m
Distance between center of mass and axle	$b_R = 0$ m
Axle cornering stiffness	$C_3 = 152$ kN/rad
Other parameters	
Passenger standard mass	$m_P = 75$ kg
Rotational damping coefficient at the pivot (linearized characteristic function of the joint)	$c_{low} = 2\times10^3 \rightarrow 10^4$ Nms/rad $c_{high} = 2\times10^4 \rightarrow 10^5$ Nms/rad
Torsional stiffness at the pivot (linearized characteristic function of the joint)	$k_{low} = 0 \rightarrow 4\times10^4$ Nm/rad $k_{high} = 10^5 \rightarrow 10^6$ Nm/rad
Front section	$S = 8.00$ m^2
Aerodynamic drag coefficient	$C_x = 1.15$

where M_z denotes the aligning torque. Assuming now:

$$\begin{aligned} &F_{x11} \cong F_{x12}, \quad F_{x11} + F_{x12} = F_{x1} \qquad F_{y11} \cong F_{y12}, \quad F_{y11} + F_{y12} = F_{y1} \\ &F_{x21} \cong F_{x22}, \quad F_{x21} + F_{x22} = F_{x2} \qquad F_{y21} \cong F_{y22}, \quad F_{y21} + F_{y22} = F_{y2} \\ &F_{x31} \cong F_{x32}, \quad F_{x31} + F_{x32} = F_{x3} \qquad F_{y31} \cong F_{y32}, \quad F_{y31} + F_{y32} = F_{y3} \end{aligned} \tag{11}$$

then the generalized forces can be written as:

$$\begin{cases} Q_x = F_{x1}\cos\delta - F_{y1}\sin\delta + F_{x2} + F_{x3}\cos\vartheta + F_{y3}\sin\vartheta - F_A \\ Q_y = F_{x1}\sin\delta + F_{y1}\cos\delta + F_{y2} - F_{x3}\sin\vartheta + F_{y3}\cos\vartheta \\ Q_\psi = F_{x1}a_F\sin\delta + F_{y1}a_F\cos\delta - F_{y2}b_F + F_{x3}d\sin\vartheta - F_{y3}(d\cos\vartheta + l_R) + M_{z1} + M_{z2} + M_{z3} \\ Q_\vartheta = F_{y3}l_R - M_{z3} \end{cases} \tag{12}$$

where F_A represents the aerodynamic drag force. Among the longitudinal ground forces, only F_{x3} is taken into account (due to traction axle on the trailer). The equations of motion are then linearized considering the lateral ground forces F_{y1}, F_{y2} and F_{y3}, neglecting the contribution of the aligning torques and imposing a fixed constant value for the forward longitudinal component of the velocity u. This yields a decoupled algebraic equation plus a system of coupled differential equations, which using state variables reads:

$$F_{x3} = F_{y1}\delta - F_{y3}\vartheta + F_A, \quad \begin{cases} m_F(\dot v + ur) - m_R(d + a_R)\dot r + m_R a_R \dot s = F_{y1} + F_{y2} + F_{y3} - F_A\vartheta \\ J_1\dot r - J_2\dot s - m_R(d + a_R)(\dot v + ur) = F_{y1}a_F - F_{y2}b_F - F_{y3}(d + l_R) + F_A d\vartheta \\ J_3\dot s - J_2\dot r + m_R a_R(\dot v + ur) + cs + k\vartheta = F_{y3}l_R \\ \dot\vartheta = s \end{cases} \tag{13}$$

where $r = \dot\psi$ and F_A is the constant aerodynamic drag (due to constant u). The linearized ground lateral forces are given as functions of the state variables by:

$$\begin{cases} F_{y1} = C_1\alpha_1 = C_1\left(\delta - \dfrac{v + a_F r}{u}\right) \\ F_{y2} = C_2\alpha_2 = -C_2\left(\dfrac{v - b_F r}{u}\right) \\ F_{y3} = C_3\alpha_3 = -C_3\left\{\dfrac{1}{u}\left[v - (d + l_R)r + l_R s\right] + \vartheta\right\} \end{cases} \tag{14}$$

In eqs. (14) the slip angles of the two axles of the front section of the vehicle (α_1 and α_2) are obtained via standard congruence equations [18], and $\alpha_3 = \alpha_R$ descends from eq. (5).

3. Stability analysis

Stability of the linearized model is studied in equilibrium configurations by means of sensitivity analysis with respect to the model's governing parameters. The complete list of parameters of the 4 dofs model is provided in Tab. 1, along with their respective values adopted for computations in the case-study herein considered. Stability maps are drawn on the basis of sets of parameter values related straight-ahead running, steady-state manoeuvres. This specific kind of manoeuvre is considered for both respecting the validity of linear behaviour of the tyres (with respect to slip angles), and avoiding input perturbations for which it would be necessary the analysis of the nonlinear model (step-steer input, change of lane). The most important parameters controlling the onset of unstable motions are identified, with particular attention to the role played by the equivalent rotational damping coefficient c and the equivalent torsional stiffness k characterizing the joint.

The model's governing parameters can be divided into two sets: manoeuvre-dependent parameters (travelling speed V_0 and cornering stiffness of the three axles C_1, C_2, C_3) and manoeuvre-independent (or vehicle-dependent) parameters (inertial parameters, geometric parameters, the equivalent rotational damping coefficient c and the equivalent torsional stiffness k characterizing the joint). The latter parameters (c, k) are obtained through linearization of the viscoelastic characteristic function of the joint.

3.1 Characteristic function of the joint

The hydraulic joint considered in this study, as typically adopted on articulated buses, consists of a mechanical joint, plus a pair of passive hydraulic cylinders connecting the front section of the vehicle with the trailer (as shown in Fig. 2). The two cylinders are interconnected by a hydraulic circuit, equipped with regulation valves (a detailed description of the joint that has been modelled is given in [24]; similar hydraulic joints for prevention of jackknifing are described in several other patents [5, 25, 26, 27, 28]). The viscoelastic behaviour of the joint is then described by a generally nonlinear characteristic function.

The viscoelastic characteristic function of the adopted joint has been numerically estimated, as reported in Figs. 3 and 4 for two possible operational modes of the joint (displaying in both cases the torque M as a function of the rotation angle ϑ, at different values of relative angular velocity). The mode in Fig. 3 is characterized by a low value of rotational viscous damping c at small angles ϑ, with no torsional stiffness, while the mode in Fig. 4 is characterized by a torsional stiffness k in parallel with respect to c at small angles ϑ.

3.2 Stability maps

Stability maps are obtained by applying the Routh-Hurwitz criterion to the characteristic equation descending from Eqs. (13), using a symbolic algebra software. A set of values is adopted for the model parameters, related to a straight-ahead running, steady-state manoeuvre, as reported in Tab. 1, along with ranges of possible variations for some of them.

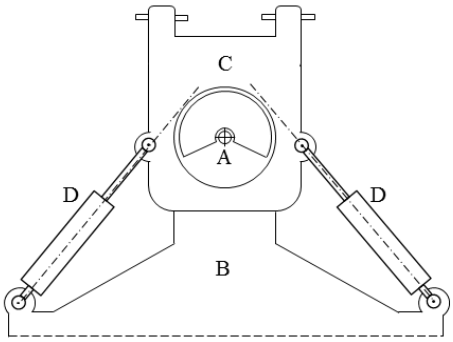

Fig. 2. Schematic of a hydraulic swivel joint adopted on articulated buses
(A = swivel axis, B = rear section or trailer, C = junction to front section, D = hydraulic cylinders).

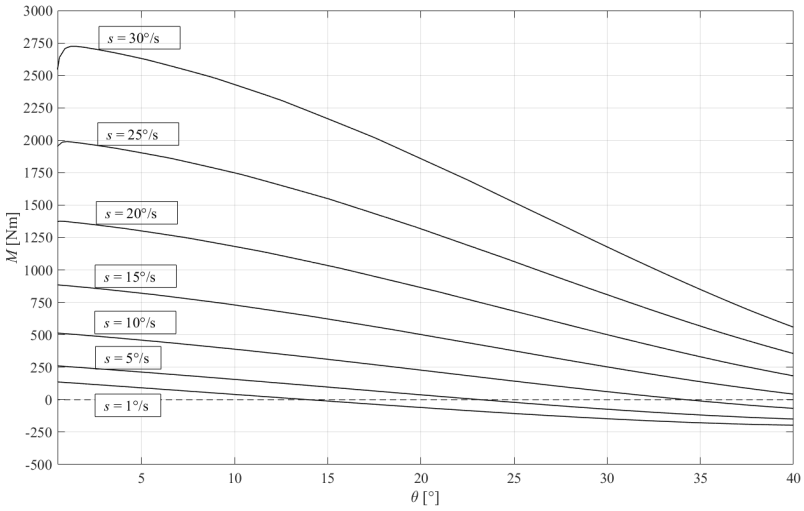

Fig. 3. Characteristic of the joint: mode with no torsional stiffness k at small ϑ, effect of angular velocity $s = \dot{\vartheta}$.

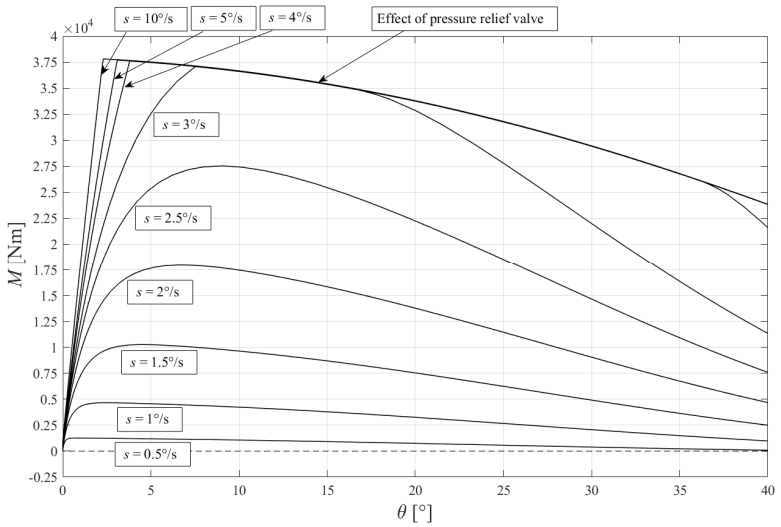

Fig. 4. Characteristic of the joint: mode with torsional stiffness k at small ϑ, effect of angular velocity $s = \dot{\vartheta}$.

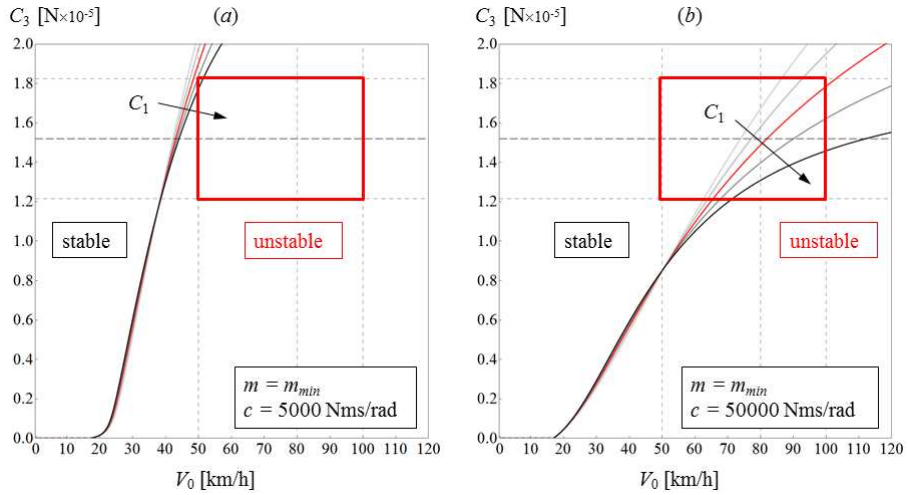

Fig. 5. Stability maps: effect of varying the cornering stiffness C_1 of the front axle with low (*a*) and high damping (*b*); case without passengers.

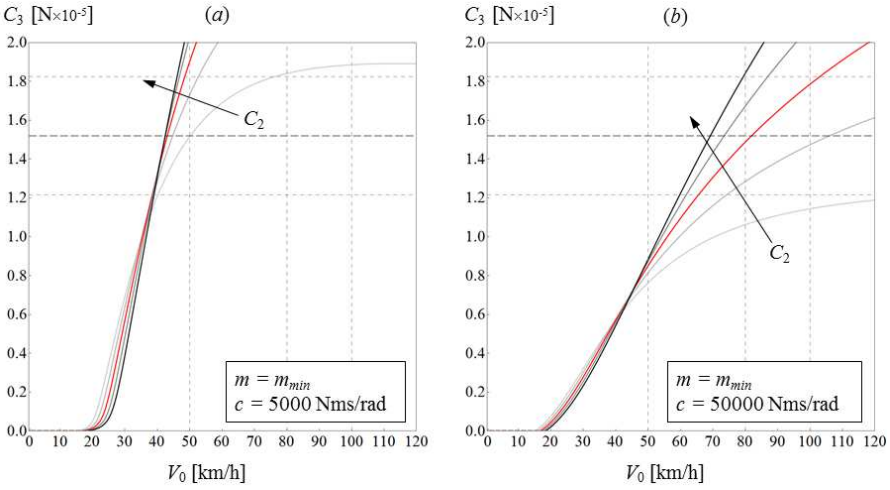

Fig. 6. Stability maps: effect of varying the cornering stiffness C_2 of the intermediate axle with low (*a*) and high damping (*b*); case without passengers.

Stability maps are drawn in the form of Cartesian diagrams depending on the two most influential manoeuvre-dependent parameters, the travelling speed V_0 and the cornering stiffness of the trailer axle C_3. Each point of a diagram represents a steady-state equilibrium point; a stability threshold separates a stable region from an unstable region; more than one stability threshold can be displayed (superimposed) on a single map, by varying a third parameter other than V_0 and C_3. In the maps, a theoretical high damping value (c_{high}) is also considered, for comparing the results with the actual value given by the linearized characteristic function of the joint (c_{low}, one order magnitude lower, as in Fig. 2). In the diagrams, the horizontal bold dashed line refers to the average value of C_3 reported in Tab. 1.

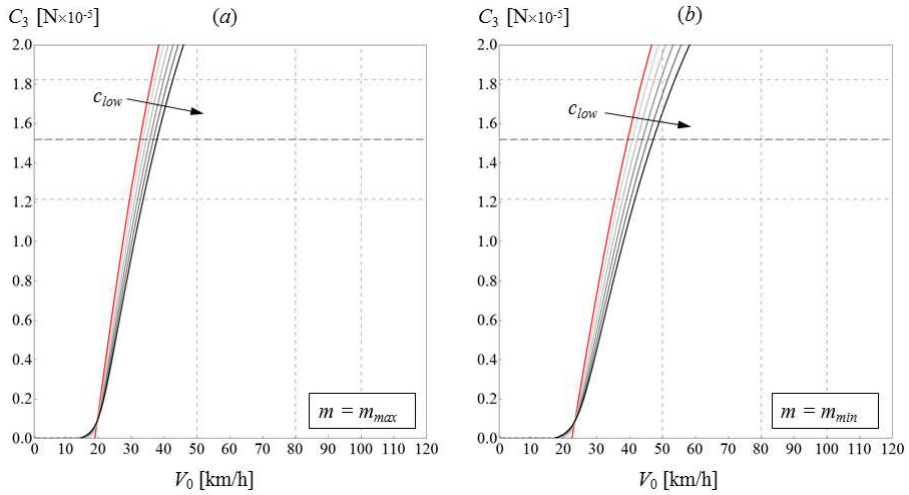

Fig. 7. Stability maps: effect of varying the equivalent rotational damping coefficient c in the low range, in the case with full load (*a*) and without passengers (*b*).

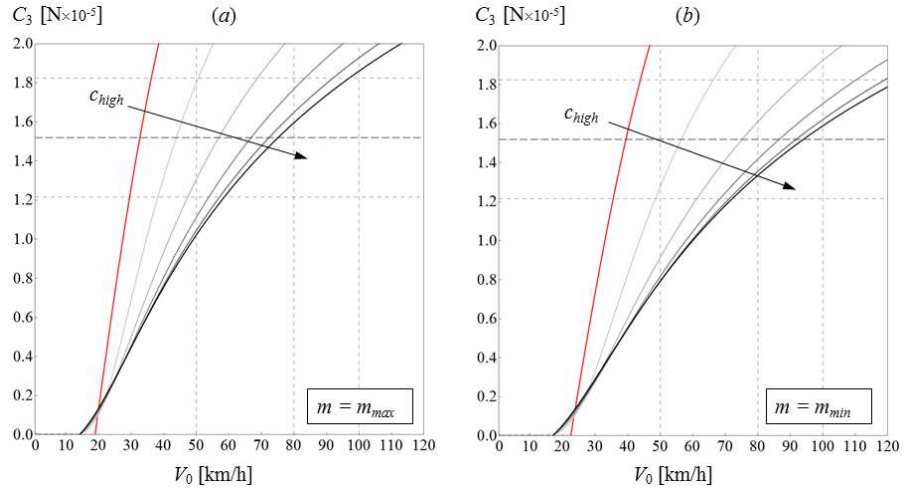

Fig. 8. Stability maps: effect of varying the equivalent rotational damping coefficient c in the high range, in the case with full load (*a*) and without passengers (*b*).

Effects of the travelling speed (V_0). Increasing the travelling speed V_0 (while keeping constant all the other parameters) has always destabilizing effects, as it can be observed in the stability maps displayed in Figs. 5-14. In particular, the stability thresholds (curves) are related to the unstable behaviour of the 'jackknifing' mode of the vehicle (Hopf bifurcation, leading to oscillatory or flutter instability); while the straight vertical thresholds (as in Figs. 9 and 10) are instead related to unstable behaviour at the critical speed of the vehicle (divergence instability).

Effects of the cornering stiffness of the axles (C_1, C_2, C_3). The effect of varying the cornering stiffness C_1 of the front axle (in the range: –20%, –10%, +0%, +10%, +20%,) in the case without passengers is shown in Fig. 5, with low damping (*a*) and high damping (*b*), where a red rectangle put in evidence the region of major interest for stability analysis within the present study. The effect of varying the cornering stiffness C_2 of the intermediate axle (in the same range as in Fig. 5) in the case without passengers is shown in Fig. 6, with low damping (*a*) and high damping (*b*). A reduction of C occurs when the normal (vertical) load on the axle (F_z) is lowered, or when the lateral load (F_y) is raised (due to non-linear behaviour in tyre characteristics). Reducing C_3 has destabilizing effects. At high values of C_3, a reduction of C_1 destabilizes (Fig. 5), while, on the opposite, an increase of C_2 destabilizes (Fig. 6).

Effects of relative pitch and roll angles. Some remarks about pitching and rolling effects can also be stated at this stage, even though the adopted model is planar. In fact, the model is sensitive to longitudinal and lateral load transfers through the values of C_1, C_2, C_3 due to the characteristic functions of the axles (depending on tyres and on suspensions). Relative pitch between the two sections of the vehicle occurs when braking or accelerating. When braking with the engine (trailer, axle 3), the longitudinal load transfer (due to inertial effects) may generate an increase of normal load on axle 2, which effect is destabilizing (Fig. 6). The opposite may happen during acceleration, which therefore would be stabilizing. Relative roll between the two sections of the vehicle would be decoupled in presence of a spherical joint. In this case, the roll angle of the trailer would be related to an increase of lateral load transfer on axle 3, lowering the cornering stiffness C_3 with more or less important destabilizing effects (Figs. 5-13). In case of non-spherical joints, before drawing conclusions about stability the lateral load transfer distribution on the three axles should be carefully assessed (depending on the roll stiffness of the axles and on the torsional stiffness of the joint with respect to the *x* axis).

Effects of viscous damping in the joint (c). The effect of varying the damping coefficient in the low range (c = 0, 2×10^3, 4×10^3, 6×10^3, 8×10^3, 10×10^3 Nms/rad) is shown in Fig. 7, in the case with full load (*a*) and without passengers (*b*). The same effect, but in the high range of the damping coefficient (c = 0, 2×10^4, 4×10^4, 6×10^4, 8×10^4, 1×10^4 Nms/rad) is shown in Fig. 8, in the case with full load (*a*) and without passengers (*b*). In addition, the effect of varying the damping coefficient in the high range (as in Fig. 8) is shown in Fig. 9*a*, in the case of front section of the vehicle without passengers and trailer with full load. At high values of C_3, the variation of viscous damping coefficient c_{low} (in the range inferred from Fig. 2) is scarcely influential, even with maximum payload (Fig. 7). Raising of one order magnitude the viscous damping coefficient up to c_{high} would be more influential (Fig. 8); however, to stabilize in all

conditions the whole region of major interest (red rectangle in Fig. 5), c should be increased to extremely high values, far beyond 10^5 Nms/rad. With respect to this problem, it should also be considered the saturation (non-linear) effect that occurs increasing c, as clearly shown in Fig. 8 (beyond a certain value of c, its increase would hardly be influential on the position of the stability threshold). In any case, the worst condition with respect to stability would be represented by a mass distribution consisting of trailer loaded by maximum payload, and front section loaded by minimum payload (as in Fig. 9*a*). It should also be noticed that high values of damping coefficient c would have the (negative) effect of enhancing the sensitivity of stability thresholds to the cornering stiffness C of the axles. This suggests that simply increasing the damping coefficient c is not a solution for the stability problem (it does not ensure stability in all conditions of interest, enhancing significantly the sensitivity of stability thresholds to manoeuvre-dependent parameters).

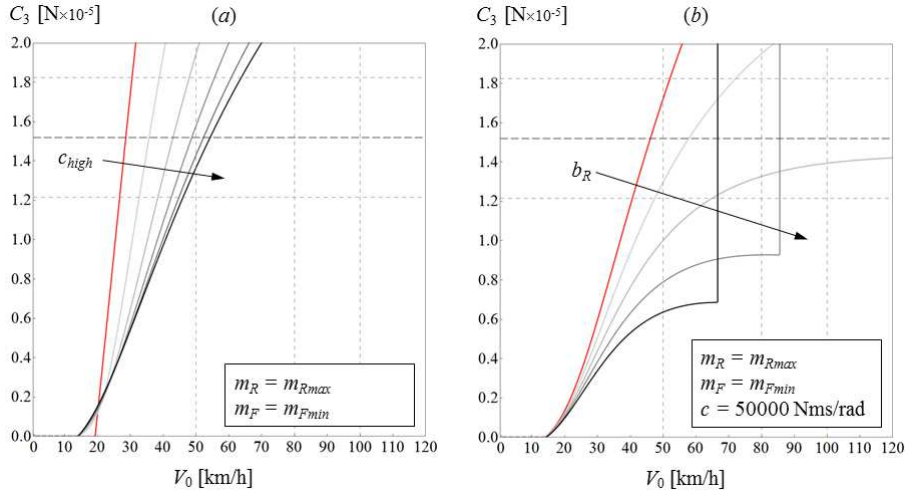

Fig. 9. Stability maps: effect of varying c in the high range (*a*), and effect of varying the distance b_R keeping l_R constant (*b*), in both cases with front section without passengers and trailer with full load.

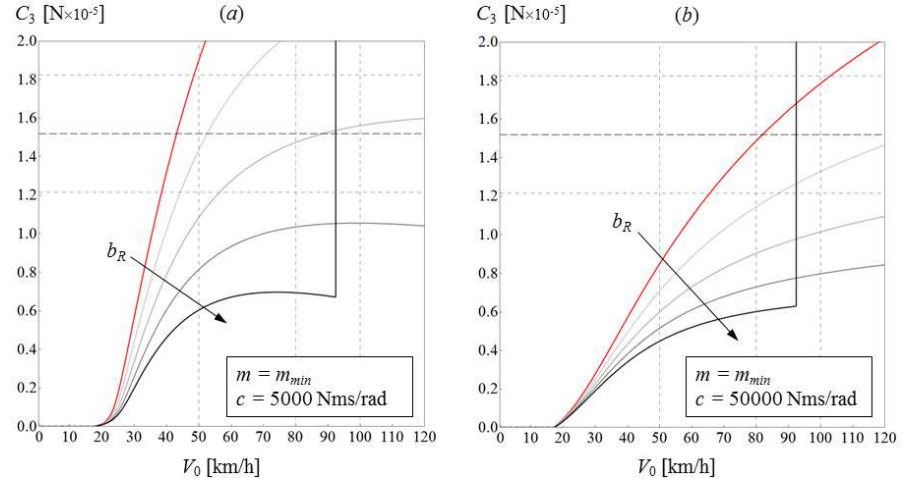

Fig. 10. Stability maps: effect of varying the distance b_R (keeping l_R constant) in the case without passengers, with low damping (*a*) and high damping (*b*).

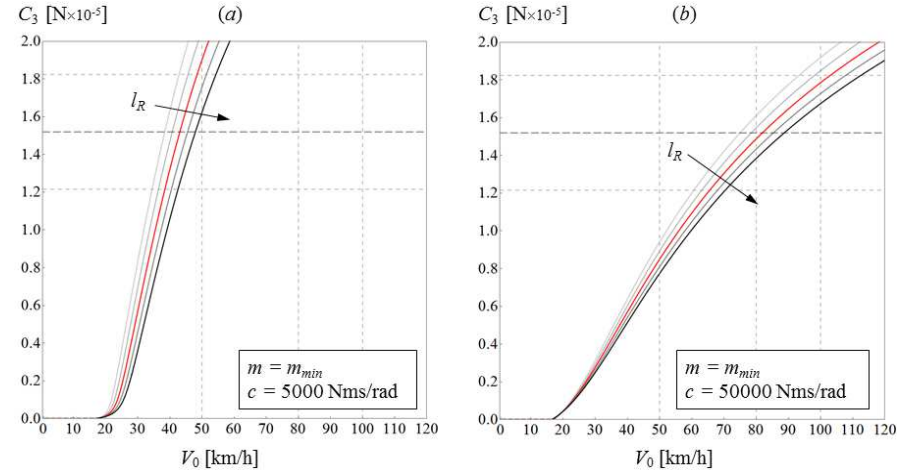

Fig. 11. Stability maps: effect of varying the distance l_R (keeping $b_R = 0$) in the case without passengers, with low damping (*a*) and high damping (*b*).

Effects of the length of the trailer and of the position of its center of mass (l_R, b_R). The effect of varying the distance b_R between the center of mass of the trailer and its axle (in the range b_R = +0%, +3%, +6%, +9%, +12% of l_R, keeping l_R constant) is shown in Fig. 9*b*, in the case of front section of the vehicle without passengers and full load trailer, with high damping. The effect of varying the distance b_R between the center of mass of the trailer and its axle (in the same range as in Fig. 9*b*, keeping l_R constant) is shown in Fig. 10, case without passengers with low damping (*a*) and high damping (*b*). The effect of varying the distance l_R between pivot and axle of the trailer (in the range: –10%, –5%, +0%, +5%, +10%, keeping b_R = 0) is shown in Fig. 11, case without passengers with low damping (*a*) and high damping (*b*).

Varying the length of the trailer l_R, while keeping constant all the other parameters, is scarcely influential (however, its increase is stabilizing: Fig. 11). On the other hand, at high values of C_3, increasing b_R (i.e. moving forward the position of the center of mass of the trailer) is strongly stabilizing (with both low and high damping coefficients, and with both minimum and maximum payload). Indeed, b_R has been identified as one of the two most influential parameters on stability, among the vehicle-dependent ones (or, in other words, the stability thresholds exhibit maximum sensitivity with respect to the position of the center of mass of the trailer). For enhancing stability, the center of mass of the trailer should not be located towards the end of the trailer: in this respect, therefore, the position of the engine at the rear of the trailer, typical of pusher articulated buses, represents a great disadvantage. Notice that with maximum payload at the trailer, it is likely that its center of mass is moved forward, with respect to its position at minimum payload. Finally, attention should be payed also to the effect of b_R on the critical speed of the model: if it is true that increasing b_R has stabilizing effects, it is also true that it reduces the critical speed, as it can be noticed in Fig. 10, and especially in Fig. 9*b*, where the mass distribution is the most unfavourable with respect to stability.

Effects of inertial properties (m, J). The effect of varying the total mass and, with the same proportion, also the moments of inertia (in the range: –10%, –5%, +0% , +5% , +10%) is shown in Fig. 12, full load case with low damping (*a*) and high damping (*b*). The same effect, but without passengers (in the same range of variation as in Fig. 12), is shown in Fig. 13, with low damping (*a*) and high damping (*b*). The effect of varying the mass and, with the same proportion, also the moment of inertia of the trailer is shown in Fig. 14*a* (considering the front section of the vehicle without passengers, and the inertial parameters of the trailer varying in the range: –10%, –5%, +0%, +5%, +10% with respect to full load conditions) and in Fig. 14*b* (considering, on the opposite, the trailer without passengers, and the inertial parameters of the front section varying in the range: –10%, –5%, +0%, +5%, +10% with respect to full load conditions), in both cases with high damping. Varying all the inertial parameters with the same rate of change (mass and moment of inertia of both trailer and front section) yield effects of minor importance (Figs. 12 and 13). On the other hand, large relative variations of inertial properties (trailer with respect to front section) are more influential. Increasing the mass of the trailer is destabilizing (Fig. 14*a*), while increasing the mass of the front section stabilizes (Fig. 14*b*). The worst condition is represented by a mass distribution consisting of trailer loaded by maximum payload, and front section loaded by minimum payload.

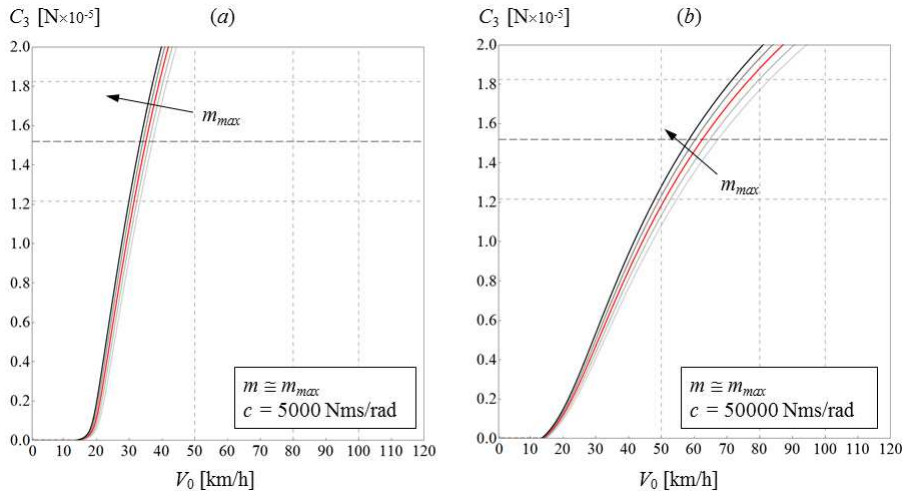

Fig. 12. Stability maps: effect of varying the total mass and the moments of inertia with low (*a*) and high damping (*b*); full load case.

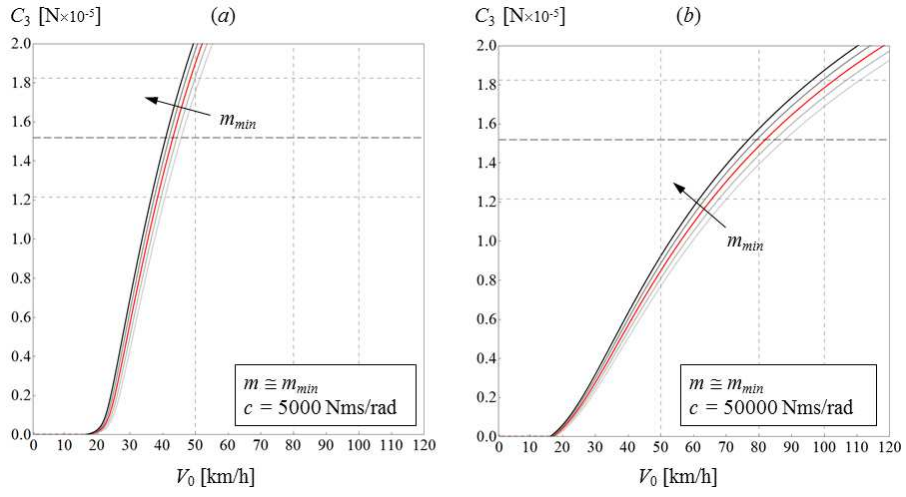

Fig. 13. Stability maps: effect of varying the total mass and the moments of inertia with low (*a*) and high damping (*b*); case without passengers.

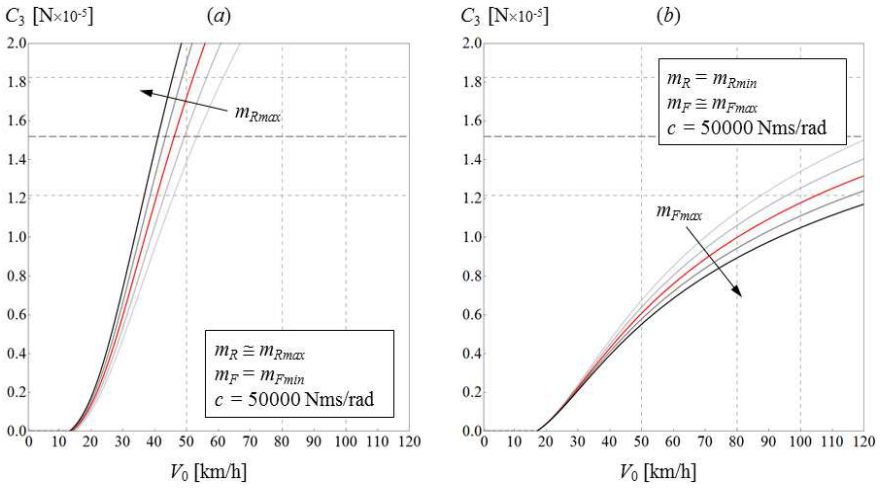

Fig. 14. Stability maps: effect of varying separately the inertial properties of the trailer (*a*) and those of the front section of the vehicle (*b*), with high damping in both cases.

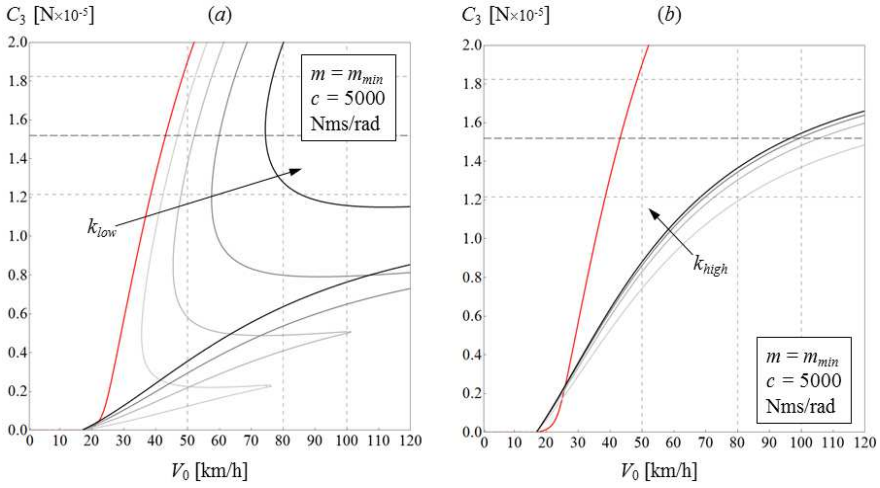

Fig. 15. Stability maps: effect of varying the equivalent torsional stiffness k in the low range (*a*) and in the high range (*b*), without passengers and with low damping in both cases.

Effects of torsional stiffness at the joint (k). Introducing a torsional stiffness k at the joint has the strongest effects in modifying the stability thresholds, affecting in particular also their shapes, as displayed in Fig. 15 (where the red threshold identifies the case at $k = 0$). In Fig. 15*a*, k varies in a low range ($k = 1\times10^4$, 2×10^4, 3×10^4, 4×10^4 Nm/rad) and in Fig. 15*b*, it varies in a high range ($k = 2.5\times10^5$, 5.0×10^5, 7.5×10^5, 10×10^5 Nm/rad), without passengers and with low damping in both cases. An angular point appears with $k \neq 0$ (Fig. 15*a*), which produces a lobe in the upper part of the map, which moves out of the bounds of the diagram at higher values of k (Fig. 15*b*). In the range of variation of major interest for C_3, an intermediate interval of values can therefore be identified for k, leading to the best operating conditions with respect to linear stability (aimed at clearing off the lobe in the upper part of the diagram, while limiting below acceptable values the whole lower branch of the stability threshold). It should also be considered the saturation (non-linear) effect that occurs increasing k, as shown in Fig. 15*b* (beyond a certain value of k, its increase is hardly influential on the position of the stability threshold; and actually it has negative effects on stability, since it broadens the instability region in the lower part of the diagram).

3.3 Analysis with a multibody model

To assess the results obtained with the single-track model, a multibody analysis of the bus under study was performed, also considering the vertical dynamics of the vehicle. The multibody model was developed within Altair MotionView (Fig. 16), while the hydraulic joint was modelled within Simulink. The data for modelling the bus, consistent to those reported in Tab. 1, are referred to Mercedes-Benz Citaro G NGT 3 (Fig. 1*a*). The model includes suspensions and steering system, and it consists of rigid bodies only: front section sprung mass, rear section (trailer, with engine and driveline) sprung mass, unsprung masses of axles 1, 2, 3, and wheels. Internal constraints were modelled by revolute joints (wheels), prismatic joints (vertical travel of suspensions) and cylindrical joints (vertical travel of front wheels). Additional parameters with respect to those given in Tab. 1 are reported in Tab. 2 (mass and size of wheels, ground equivalent damping and ground equivalent stiffness of suspensions, with related preloads).

Straight-ahead running manoeuvres were simulated in ideal conditions, considering perfectly symmetric tyres and suspensions on both sides of the vehicle. Therefore the model is not affected by handling anomalies caused by tolerances [19, 20], meaning that the only deviations with respect to the straight trajectory are due to external actions. The latter consist of ground contact forces and aerodynamic forces. The ground contact forces were modelled according to a brush model, in pure slip conditions (steady-state straight-ahead running manoeuvre, linear behaviour of the tyres). The cornering stiffness of the axles are reported in Tab. 1, while both self-aligning torques and camber thrusts were disregarded. The aerodynamic forces consist of the drag resultant force (simpler to model, with respect to the case of articulated trucks [21]), plus a fictitious lateral wind gust. The latter was simulated as an impulsive force for exciting oscillations, applied after the system has reached steady-state travelling conditions. This fictitious force (say F_{LWG}) is applied to the trailer only:

$$F_{LWG} = \frac{1}{2}\rho C_A A v_w^2 \tag{15}$$

where ρ is the air density (ρ = 1.225 kg/m^3), C_A is an aerodynamic coefficient (C_A = 2), A is the lateral surface of the trailer and v_w is the velocity of wind. The latter is set in order to obtain F_{LWG} = 1000 N, sufficient to excite small lateral oscillations, and in any case not large enough to produce wheel detachment or overturning.

Complete sets of numerical simulations were performed, varying in the ranges of interest all the parameters affecting stability (a few examples are displayed in Figs. 17, 18 and 19). The results are in full agreement with those obtained with the single track model, which is therefore able to describe correctly the stability behaviour of the vehicle (within the manoeuvre considered, for small oscillations), and it is able to identify all the main parameters controlling the onset of instability.

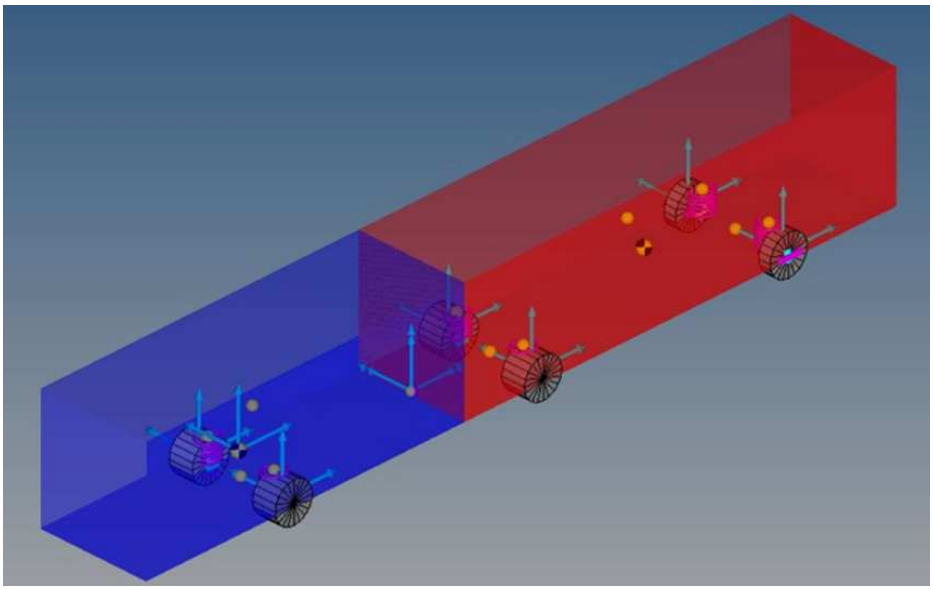

Fig. 16. Graphical representation of the multibody model.

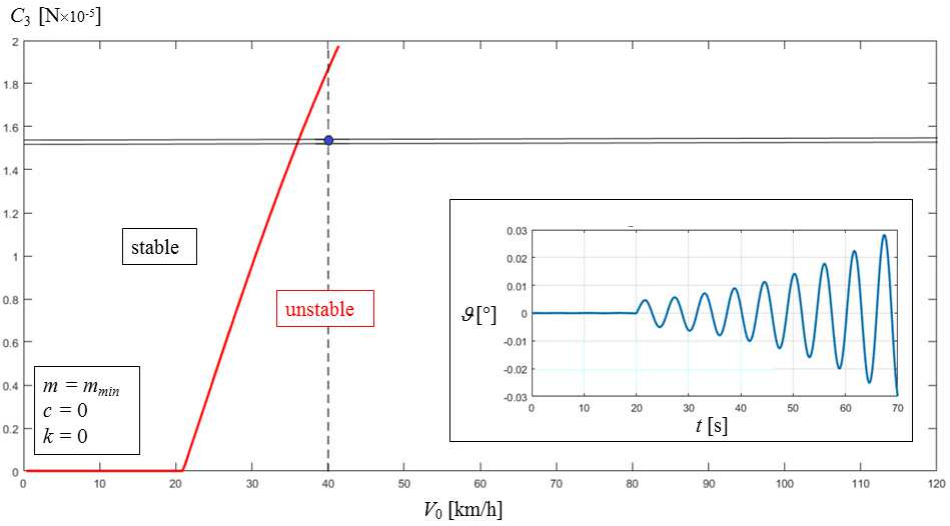

Fig. 17. Simulated manoeuvre: unloaded bus, V_0 = 40 km/h, c = 0, k = 0 (oscillating instability).

Table 2. List of additional parameters for the multibody model.

Wheels			
Axle	*Mass (one wheel)* [kg]	*Radius* [mm]	*Width* [mm]
1 (front)	60	447	275
2 (rear)	90 (twins)	447	550 (twins)
3 (trailer)	90 (twins)	447	550 (twins)
Suspensions			
Axle	*Stiffness* [N/m]	*Preload* [N]	*Damping* [Ns/m]
1 (front)	6×10^5	25×10^3	8×10^3
2 (rear)	3×10^5	30×10^3	16×10^3
3 (trailer)	3×10^5	30×10^3	16×10^3

In Figs. 17, 18 and 19 it is possible to observe the onset of both oscillating and divergence instability. The multibody model analysis confirms that the role of the suspensions is that of modifying the characteristic functions of the axles: no relevant additional effects with respect to the single-track model analysis was observed. It also confirms that damping in the joint is not able to prevent divergence instability, however it can delay its occurrence, leaving time to the driver to control it. The role of the stiffness in the joint also in this case is very influential, and at high values of the stiffness constant k, a divergence instability is detected (Fig. 19).

4. Discussion

The most important parameters controlling the onset of unstable motions in a pusher articulated bus travelling on a straight line at constant speed were identified with the aid of a set of stability maps, assessing the results by a multibody analysis. Pusher articulated buses present a great disadvantage in terms of mass distribution, due to the position of the engine at the rear of the trailer. In fact, for enhancing stability, the center of mass of the trailer should not be positioned towards the end of the trailer. Regarding mass distribution, it should also be mentioned that the worst condition with respect to stability was identified by trailer loaded by maximum payload, and front section loaded by minimum payload.

New results were found about the ability of the viscoelastic joint in controlling the stability of the vehicle. As for the equivalent rotational damping coefficient c, it was found to have the negative effect of enhancing the sensitivity of the stability thresholds to the cornering stiffness of the axles; even with very high damping values, the stability region would not include the whole area of major interest, which suggests that simply increasing the damping coefficient is not a solution for the stability problem. As for the torsional stiffness k, it was found to have the strongest effects in modifying the stability thresholds, affecting in particular also their shapes; an optimal interval of values can be identified for k, leading to the best operating conditions with respect to stability within the analysis of the linearized system.

The next step in the present study shall be its extension to consider nonlinearities arising from tyres and kinematical terms in the equations of motion, and then performing bifurcation analysis for investigating the post-critical stability by means of an appropriate perturbation method [32]. In fact, it is already known that for moderate to high forward speeds at least a sub-critical Hopf bifurcation occurs [11]. This means that for sufficiently large disturbances linearly stable motions may diverge and become unbounded, which happens due to an unstable limit cycle at speeds less than the critical value (i.e. the domain of attraction for the stable equilibrium position is bounded by an unstable limit cycle [14]). For design and control purposes, it will be of great importance studying the amplitude of such limit cycles as functions of driving parameters of the model, and in particular of the viscoelastic ones characterizing the hydraulic joint.

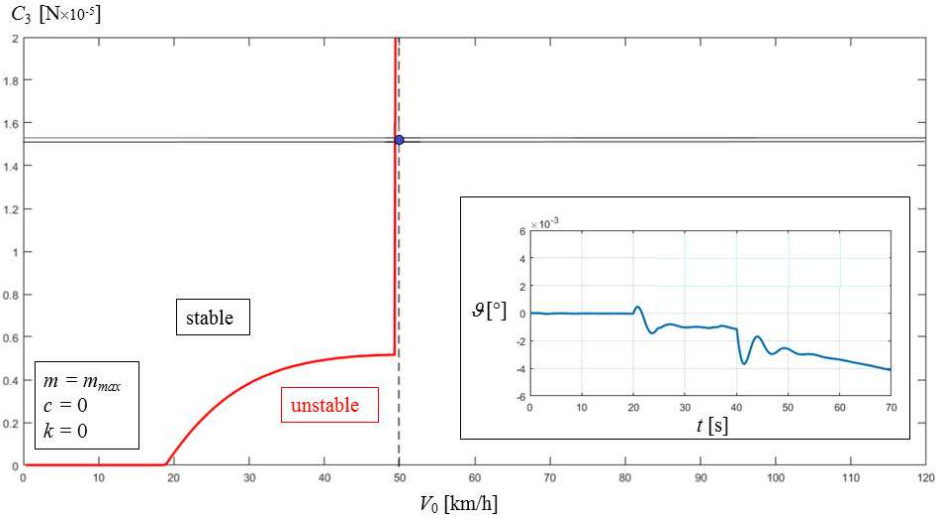

Fig. 18. Simulated manoeuvre: fully loaded bus, V_0 = 50 km/h, c = 0, k = 0 (divergence instability).

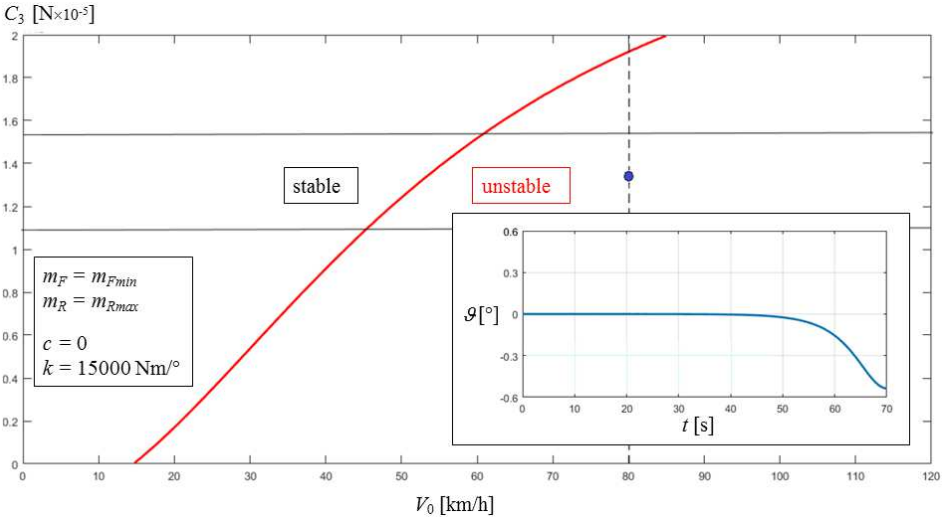

Fig. 19. Simulated manoeuvre: unloaded front section, fully loaded trailer, V_0 = 80 km/h, c = 0, k = 15000 Nm/° (divergence instability).

5. Conclusion

A new contribution was given on the linear stability of articulated vehicles, considering the peculiar features of a pusher articulated bus equipped with hydraulic joint. The most important parameters controlling the onset of unstable motions were identified by thoroughly investigating straight-ahead running, steady-state manoeuvres by means of a set of stability maps. Particular attention was payed to study the role played by the equivalent rotational damping coefficient and the equivalent torsional stiffness characterizing the joint, with the aim of finding general criteria for its design. It was found that pusher articulated buses present a great disadvantage in terms of mass distribution, due to the position of the engine at the rear of the trailer. Moreover, simply increasing the damping coefficient of the joint is not a solution for the stability problem, since even with very high damping values, the stability region would not include the whole area of interest. On the other hand, the rotational stiffness of the joint has the strongest effects in modifying the stability thresholds; an optimal interval of values can therefore be identified for k, leading to the best operating conditions. It can be concluded that the equivalent visco-elastic characteristic function of the joint plays a role of paramount importance in stability control of this particular kind of articulated vehicle. Future work shall develop bifurcation analysis for studying the post-critical behaviour of the nonlinear model. For design and control purposes, it will be of great importance studying the limit-cycle amplitudes as functions of the viscoelastic parameters characterizing the hydraulic joint.

Author Contributions

A. De Felice contributed to developing the mathematical models and performed the computations; M. Mercantini contributed to modelling the hydraulic system and to develop the multibody model; S. Sorrentino initiated the project and contributed to developing the models. The manuscript was written through the contribution of all authors. All authors discussed the results, reviewed, and approved the final version of the manuscript.

Acknowledgments

Protezioni Elaborazioni Industriali (PEI) Srl is kindly acknowledged for having supported the present study. Attilio Di Nunno and Felice Napolitano of PEI are also kindly acknowledged for their valuable contribution.

Conflict of Interest

The authors declared no potential conflicts of interest with respect to the research, authorship, and publication of this article.

Funding

The authors received no financial support for the research, authorship, and publication of this article.

Nomenclature

A	Lateral surface area	m	Mass
a_F	Front wheelbase of front section	N	Maximum number of passengers
a_R	Distance between pivot and center of mass of trailer	Q	Generalized force
b_F	Rear wheelbase of front section	r	Yaw velocity of front section
b_R	Rear wheelbase of trailer	S	Front section area
$C_{1,2,3}$	Cornering stiffness of axles 1,2,3	T	Kinetic energy
C_A	Lateral aerodynamic coefficient	t	Track
C_x	Aerodynamic drag coefficient	u	Longitudinal velocity component
c	Viscous damping coefficient (hydraulic joint)	v	Lateral velocity component
d	Distance between center of mass and pivot	v_w	Air velocity of lateral wind gust
F	Force	X,Y	Coordinates of inertial reference system
G	Center of mass	x,y	Coordinates of local reference systems
J	Mass moment of inertia	α	Slip angle
k	Torsional stiffness (hydraulic joint)	δ	Steering angle
L	Work	θ	Relative angle with trailer
l_F	Wheelbase of front section	ρ	Air density
l_R	Distance between pivot and axle of the trailer	ψ	Yaw angle

References

[1] Wei, L., Hongwen, H., Fenchun, S., Jiangyi, L., Integrated chassis control for a three-axle electric bus with distributed driving motors and active rear steering system, *Vehicle System Dynamics*, 55(5), 2017, 601-625.
[2] Fragassa, C., Electric city buses with modular platform: a design proposition for sustainable mobility, in: Campana, G., et al. (eds), *Sustainable Design and Manufacturing 2017 (SDM 2017), Smart Innovation, Systems and Technologies 68*, Springer, Cham, Switzerland, 14.1, 789-800, 2017.
[3] Van de Molengraft-Luijten, M.F.J., Besselink, I.J.M., Verschuren, R.M.A.F., Nijmeijer, H., Analysis of the lateral dynamic behaviour of articulated commercial vehicles, *Vehicle System Dynamics*, 50(1), 2012, 169-189.
[4] Aurell, J., Winkler, C.B., Standard Test Procedures for the Lateral Stability of Heavy Vehicle Combinations, *Road Transport Technology*, 4, 463-471, 1985.
[5]I. Ratskó, J. Ivony, J. Mádi, G. Karász, US Patent 4.344.640, 1982.
[6] Fancher, P.S., Winkler, C., Directional performance issues in evaluation and design of articulated heavy vehicles, *Vehicle System Dynamics*, 45(7-8), 2007, 607-647.
[7] Genta, G., *Motor Vehicle Dynamics: Modeling and Simulation*, World Scientific Publishing, Singapore, 1997.
[8] Pacejka, H.B., *Tyre and Vehicle Dynamics*, Butterworth-Heinemann, Oxford, 2002.
[9] Leipholz, H., *Stability theory, an introduction to the stability of dynamic systems and rigid bodies*, Wiley-Teubner, Stuttgart, 1987.
[10] Beregi, S., Takács, D., Stépán, G., Tyre induced vibrations of the car–trailer system, *Journal of Sound and Vibration*, 362, 2016, 214-227.
[11] Tousi, S., Bajaj, A.K., Soedel, W., Closed-loop directional stability of car-trailer combinations in straight-line motion, *Vehicle System Dynamics*, 21(1), 1992, 333-360.
[12] Kaçani, V., Stribersky, A., Troger, H., Maneuverability of a truck-trailer combination after loss of stability, *Vehicle System Dynamics*, 17(1), 1988, 186-198.

[13] Peng, T., *et al*., Bifurcation of lane change and control on highway for tractor-semitrailer under rainy weather, *Journal of Advanced Transportation*, 2017, Article ID 3506053.
[14] Troger, H., Zeman, K., A non-linear analysis of the generic types of loss of stability of the steady-state motion of a tractor semi-trailer, *Vehicle System Dynamics*, 13, 1984, 161-172.
[15] Ding, N., Shi, X., Zhang, Y., Chen, W., Analysis of bifurcation and stability for a tractor semi-trailer in-planar motion, *Vehicle System Dynamics*, 52(12), 2014, 1729-1751.
[16] Odhams, A.M.C., Roebuck, R.L., Jujnovich, B.A., Cebon, D., Active steering of a tractor semi-trailer, *Proceedings of the Institution of Mechanical Engineers, Part D: Journal of Automobile Engineering*, 225, 2011, 847-869.
[17] Zhou, S.W., Jackknife Control on Tractor Semi-trailer during High Speed Curve Driving, *Proceedings of the Institution of Mechanical Engineers, Part D: Journal of Automobile Engineering*, 225, 2011, 28-42.
[18] Rusev, R., Ivanov, R., Staneva, G., Kadikyanov, G., A study of the dynamic parameters influence over the behavior of the two-section articulated vehicle during the lane change manoeuvre, *Transport problems*, 11(1), 2016, 29-40.
[19] Krumpholc, T., Barton, S., Driver's influence on kinematics of articulated bus, *Acta Universitatis Agriculturae et Silviculturae Mendelianae Brunensis*, 61(3), 2013, 683-689.
[20] Dang, H.A., Kovanda, J., Determination of trajectory of articulated bus turning along curved line, *Transactions on Transport Sciences*, 7(1), 2014, 35-44.
[21] Leonelli, L., Cattabriga, S., Sorrentino, S., Driveline instability of racing motorcycles in straight braking manoeuvre, *Proceedings of the Institution of Mechanical Engineers, Part C: Journal of Mechanical Engineering Science*, 232(17), 2018, 3045-3061.
[22] Cattabriga, S., De Felice, A., Sorrentino, S., Patter instability of racing motorcycles in straight braking manoeuvre, *Vehicle System Dynamics*, 59 (1), 2021, 33-55.
[23] Guiggiani, M., *The Science of Vehicle Dynamics*, Springer, New York, 2014.
[24] R. Ahrens, J.H. Dicke, U. Bittrof, J. Karasek, Europäisches Patentamt, Patentschrift EP 2 738 071, 2012 (in German).
[25] D. Scarpatetti, Deutsches Patentamt, Patentschrift DE 27 41 120, 1979 (in German).
[26] F. Hagin, J. Pausenberger, H. Drewitz, Deutsches Patentamt, Patentschrift DE 29 45 441, 1984 (in German).
[27] B. Reichl, R. Maurath, D. Koch, G. Hametner, US Patent 4.616.841, 1986.
[28] A. Pazian, D.V. Cardia, R.A. Moita, UK Patent Application GB 2515900, 2015.
[29] De Rosa, M., De Felice, A., Fragassa, C., Sorrentino, S., Passenger car steering pull and drift reduction considering suspension tolerances, *9th IRMES - Research and Development of Mechanical Elements and Systems*, Kragujevac, Serbia, *IOP Conference Series: Materials Science and Engineering*, 659(1), 012076, 2019.
[30] De Rosa, M., De Felice, A., Grosso, P., Sorrentino, S., Straight path handling anomalies of passenger cars induced by suspension component and assembly tolerances, *International Journal of Automotive and Mechanical Engineering*, 16(3), 2019, 6844-6858.
[31] Terrance, C., Zhiyin, Y., Yiling, L., Assessment of drag reduction devices mounted on a simplified tractor-trailer truck model, *Journal of Applied and Computational Mechanics*, 7(1), 2021, 45-53.
[32] Moatimid, G.M., Elsabaa, F.M.F., Zekry, M.H., Approximate solutions of coupled nonlinear oscillations: stability analysis, *Journal of Applied and Computational Mechanics*, 7(2), 2021, 382-395.

ORCID iD

Alessandro De Felice https://orcid.org/0000-0001-9142-1334
Matteo Mercantini https://orcid.org/0000-0002-8626-0836
Silvio Sorrentino https://orcid.org/0000-0003-2136-5538

How to cite this article: De Felice A., Mercantini M., Sorrentino S. Stability Analysis of Articulated Bus in Straight-ahead Running Manoeuvre, *J. Appl. Comput. Mech.*, 7(3), 2021, 1649–1662. https://doi.org/10.22055/JACM.2021.36566.2869